Journal of Renewable Materials

Tech Science Press

DOI: 10.32604/jrm.2023.026923

ARTICLE

Efficient Use of Steel Slag in Alkali-Activated Blast Furnace Slag Based Geopolymer

Yu Bai, Lei Wang and Ying Fang*

College of Materials Science and Engineering, Nanjing Tech University, Nanjing, 211816, China

*Corresponding Author: Ying Fang. Email: powderfang@163.com

Received: 03 October 2022 Accepted: 30 December 2022 Published: 07 June 2023

ABSTRACT

Energy shortage and the emission of greenhouse gases have become a global problem of urgent concern. Therefore, there is an urgent need to develop a low carbon building material. Geopolymers have become a hot topic due to their environmental sustainability and the feasibility of immobilizing industrial waste. In this paper, steel slag (SS) fines were investigated as auxiliary materials of blast furnace slag (BFS) based geopolymer. The hydration heat properties, flowability, compressive strength, sorptivity coefficient, X-ray diffraction (XRD), and scanning electron microscopy (SEM) of the geopolymer pastes were determined. The results showed that the incorporation of SS weakened the reactivity of the BFS-based geopolymer paste and improved the flow values of the paste. The compressive strength of the geopolymer with 20% SS content reached 117 MPa at 28 d. The geopolymer specimens with high compressive strength showed a low sorptivity coefficient. The microscopic results showed that the addition of the appropriate amount of SS reduced the cracks, improved the density of the geopolymer, and produced a geopolymer composite with excellent mechanical properties.

KEYWORDS

Blast furnace slag; steel slag; geopolymer; alkali-activated

1 Introduction

Energy shortage and the emission of greenhouse gases have become a global problem of urgent concern. Therefore, there is an urgent need to develop a low carbon building material. Geopolymers have become a hot topic due to their environmental sustainability and the feasibility of immobilizing industrial waste. In this paper, steel slag (SS) fines were investigated as auxiliary materials of blast furnace slag (BFS) based geopolymer. The hydration heat properties, flowability, compressive strength, sorptivity coefficient, X-ray diffraction (XRD), and scanning electron microscopy (SEM) of the geopolymer pastes were determined. The results showed that the incorporation of SS weakened the reactivity of the BFS-based geopolymer paste and improved the flow values of the paste. The compressive strength of the geopolymer with 20% SS content reached 117 MPa at 28 d. The geopolymer specimens with high compressive strength showed a low sorptivity coefficient. The microscopic results showed that the addition of the appropriate amount of SS reduced the cracks, improved the density of the geopolymer, and produced a geopolymer composite with excellent mechanical properties.

Ordinary Portland Cement (OPC) is still the most widely used building material, and the world produces about 4 billion tons of cement each year. However, the production of OPC requires significant resources and releases a lot of CO_2. According to statistics, for every ton of cement produced, about one ton of CO_2 is released [1]. Its production releases about 5% of the world's CO_2 emissions [2]. Therefore, it is necessary to develop a low-carbon sustainable building material.

Geopolymers as potential alternatives to OPC have been extensively studied in recent decades [3]. Geopolymers have higher mechanical properties, better durability, excellent immobilization of heavy metals, and less CO_2 emission [4–8]. Compared to OPC, geopolymers can be reduced by 44%–64% in CO_2 emissions during preparation and 7%–39% in financial costs [9]. Geopolymer is the product of the geopolymerization of aluminum-silicate raw materials and alkali activators. The geopolymerization process can be divided into several steps: (1) dissolution of Al and Si from the solid material in a highly concentrated alkaline solution, (2) formation of Si-Al oligomers, (3) polycondensation of the oligomers to form Si-Al polymers, and (4) further polycondensation, resulting in the formation of a hardened geopolymer solid [10]. The sources of precursor raw materials used in geopolymers vary, whether natural products or industrial wastes are required to be rich in alumina and silica content, preferentially in amorphous form. In recent years, materials such as fly ash [11], blast furnace slag [12], metakaolin [13], rice husk ash [14], and high-titanium slag [15] have been widely used in geopolymers. However, the range of precursor materials is still increasing with the continuous utilization of resources.

Steel slag (SS) is the industrial solid waste discharged during steelmaking. In 2019, global crude steel production reached 18688.8 million tons, of which China produced 996.3 million tons, accounting for more than 50% of the total, making China the world's largest steel producer [16]. The re-utilization rate of SS in China (only about 50%) [17] is lower than in countries such as Japan (98.4%) [18], the EU (87%) [19], and the US (84.4%) [20]. The main reasons restricting the mass utilization of steel slag are its complex composition and low early activity (low content of active minerals C_3S, and C_2S) [21,22]. Therefore, further development of the effective utilization of steel slag and increasing its added value has become an issue of concern, and the use of SS instead of other pozzolanic materials to prepare geopolymer is a suitable approach. Blast furnace slag (BFS) has great potential for applications in geopolymer preparation due to its chemical composition and high reactivity [23]. The use of blast furnace slag for geopolymer precursors has been widely reported. Saludung et al. investigated the effect of different curing methods on the high-temperature resistance of fly ash-slag-based geopolymer [24]. Liu et al. prepared geopolymer materials with excellent properties using Utilizing recycled powder instead of slag [25]. Huo et al. evaluated the role of two nanomaterials in the early reaction kinetics of slag-based geopolymers [26]. Lv et al. investigated the effect of curing time and percentage of material dosing on the properties of loess-slag-based geopolymer composite [27].

Although there have been many studies on blast furnace slag-based geopolymer, very few studies explore the impact of SS when used alone in based geopolymer. In this work, SS powder was added to BFS powder to compose steel slag-blast furnace slag-based geopolymer composites with excellent properties, which help to improve the reuse of both materials. Five groups of geopolymer pastes were prepared by activating binary blends of BFS and SS with an alkaline solution, and the effects of varying SS replacement levels on the micro- and macro-characterizations of BFS-based geopolymer pastes were investigated to provide the necessary data for further research and utilization of SS.

2 Experimental Program

2.1 Materials

The BFS and SS used in this experiment were obtained from steel companies in Zhengzhou, Henan, Province (China), and Jincheng, Shanxi Province (China). The compositions of BFS and SS are shown in Table 1. The major oxide composition of BFS is SiO_2, CaO, and Al_2O_3, and the main oxide composition

of SS is SiO_2, CaO, and Fe_2O_3. Fig. 1 shows SEM images of the BFS and SS powders. The shape of BFS and SS was irregular, with well-defined edges, as observed by scanning electron microscopy. Fig. 2 shows the particle size distribution measured by the Malvern Mastersizer 2000 laser particle size analyzer. The average particle size of BFS powder is $D_{50} = 12.461$ μm, and the average particle size of SS powder is $D_{50} = 15.767$ μm.

Table 1: Chemical compositions of BFS and SS w/%

Oxide	SiO_2	CaO	Al_2O_3	MgO	Fe_2O_3	MnO	TiO_2	Na_2O	LOI
BFS	34.72	36.26	14.76	7.62	0.806	0.48	1.01	0.765	1.58
SS	19.72	33.84	5.61	7.03	22.84	7.24	1.00	0.123	−1.01

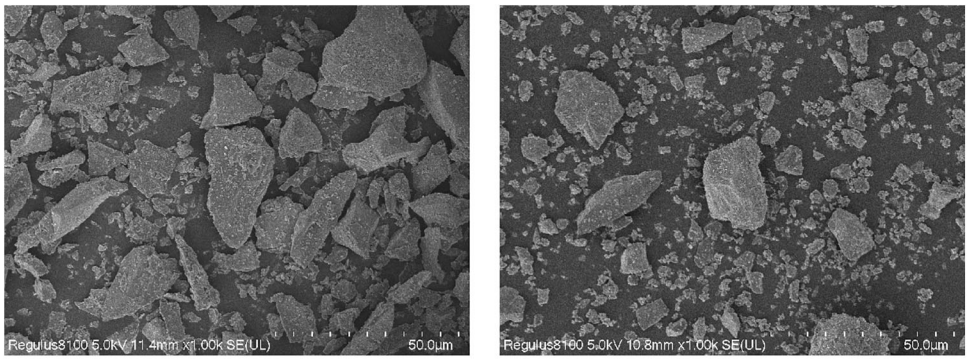

(a) (b)

Figure 1: The micrographs of (a) BFS, (b) SS

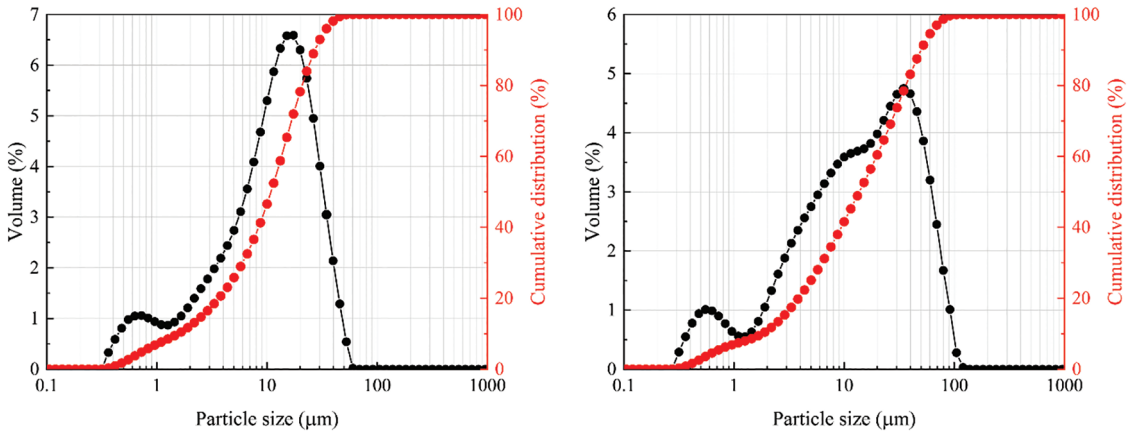

(a) (b)

Figure 2: Particle size distribution curves of (a) BFS and (b) SS

The water glass used in the experiment was supplied by Wuxi Yatai United Chemical Co., Ltd. (China) and was an industrial-grade sodium silicate water glass with an initial modulus of 2.3, consisting of 29.2% SiO_2, 12.8% Na_2O, and 60% H_2O. Due to its high silicon oxide content and high viscosity of the solution, it

is not easy to use in this experiment. The modulus of sodium silicate is adjusted to 1.5 and the concentration is 35% by adding sodium hydroxide and deionized water, and the alkaline solution should be aged for 24 h before use.

2.2 Mix Proportions

BFS was used as the basic raw material and replaced with SS according to different replacement levels. The SS content was 0%, 10%, 20%, 30%, and 40%, respectively. The mixtures were expressed as SS0, SS10, SS20, SS30, and SS40, respectively. As shown in Table 2.

Table 2: Mix proportion of BFS-based geopolymer including SS

Sample ID	Raw material		Alkaline activator			W/B
	BFS (g)	SS (g)	Modified sodium silicate solution (g)	Modulus	Additional water (g)	
SS0	100	0	40.97	1.5	14.03	0.55
SS10	90	10	40.97	1.5	14.03	0.55
SS20	80	20	40.97	1.5	14.03	0.55
SS30	70	30	40.97	1.5	14.03	0.55
SS40	60	40	40.97	1.5	14.03	0.55

The BFS and SS powders were weighed according to the test protocol and mixed thoroughly for 5 min. Then, the alkaline solution was added to the powder according to the liquid-solid ratio of 0.55 and mixed for 4 min with a rotary mixer to form homogenous geopolymer pastes. Afterward, the geopolymer pastes were poured into 20 mm × 20 mm × 20 mm cubical molds and vibrated for 1 min by a vibration table to exclude the air bubbles in the pastes to increase the compactness. The samples after vibration were sealed with plastic film and left to stand for 24 h in a laboratory environment (95% relative humidity, 25°C ± 2°C). The demolded samples were fully reacted with alkaline solution at 40°C under water curing conditions for subsequent testing.

3 Test Items and Methods

3.1 Hydration Heat

According to Chinese GB/T 12959-2008 standard [28], the roles of SS on the heat release of geopolymerization were evaluated by SHR-16 cement hydration heat tester. The hydration heat release rate of geopolymer paste within the first 72 h was measured, and the cumulative heat curve was calculated and plotted.

3.2 Flowability

The flowability test for geopolymer paste was performed based on the Chinese GB/T 8077-2012 specifications [29]. The flow cone mold (d_{top} = 36 mm, d_{bottom} = 60 mm, h = 60 mm) was placed in the center of a 500 mm × 500 mm glass plate. The fresh pastes were filled into the flow cone immediately after the completion of raw material mixing, and then the mold was lifted vertically upward. The diameters of the paste in both vertical directions were measured after 30 s, and the average of the measured values was obtained.

3.3 Compressive Strength

Based on Chinese GB/T 17671-1999 specifications [30], the mechanical properties of the cubic specimens (20 mm^3 × 20 mm^3 × 20 mm^3) were measured by using a YAW-4305 Compression Testing

Machine. The loading rate of the machine was set to 2400 ± 200 N/s, and the average value and corresponding error bars of each group were determined by measuring six replicate specimens.

3.4 Sorptivity Coefficient

The sorptivity test was based on the ASTM C1585 [31]. The specimens at the age of 28 d were dried in an oven at 50°C ± 5°C until the mass was constant. Sealant was applied around the specimen to make it permeable to water only at the bottom. The specimen was then placed in the water vertically to keep the water level at 2 mm above the bottom. After immersing the specimen in water, it was weighed at different times with intervals of 0, 1, 2^2, 3^2, 4^2, 5^2, 6^2, 7^2, 8^2, and 10^2 min. The test results were averaged to calculate the water absorption volume and then normalized for the cross-sectional area of the bottom surface of the specimen. The sorptivity coefficient was evaluated according to Eq. (1):

$$Q/A = K\sqrt{t} \tag{1}$$

where Q = volume of water absorption (mm^3), A = specimen bottom area (mm^2), t = immersion time (min), and K = water absorption coefficient ($mm/min^{1/2}$).

3.5 Microstructural Properties

Microstructural analysis of the hardened geopolymer pastes at 28 d was performed by XRD and SEM. The geopolymer specimens required for testing were collected and immersed in anhydrous ethanol to terminate their hydration reactions. Then the specimens were dried in an oven at 50°C ± 5°C until there was no reduction in specimen mass.

After drying, the specimen was ground into a fine powder (≤74 μm) and the powder was taken as the XRD test specimens. XRD tests were performed using a Rigaku Smart Lab X-ray powder diffractometer with Cu target, voltage 3 kw, XRD scan range of 5°–80°, step size 0.02°, and scan speed of 10°/min.

To observe the microscopic morphology of the geopolymer, thin-flake specimens with flat surfaces were taken, and a gold film of about 10 nm was sprayed on the surface of the specimens to be tested using a vacuum coater to enhance the electrical conductivity of the specimens, and a Hitachi Regulus 8100 SEM was used to observe the microscopic morphology of the specimens.

4 Results and Discussion

4.1 Hydration Heat

The hydration heat curves of the geopolymer pastes with varying SS contents are shown in Fig. 3. Similar to the exothermic process of hydration of cement. Its hydration process can be divided into five stages: the rapid exothermic stage, the dormant stage with low exothermic rate, the hydration acceleration stage, the hydration deceleration stage, and the steady stage [32], except that the acceleration trend was less pronounced. Fig. 3a shows the hydration exothermic rate curve of the geopolymer paste, it can be seen that the curves have two different exothermic peaks, and the maximum exothermic peak of geopolymer paste occurs at 6~8 min, which is related to the dissolution of BFS and SS powder into SiO_2 and Al_2O_3 monomer in alkali solution [33]. After the dormant period, the thermal evolution curve of the geopolymer paste shows a small second exothermic peak, which is mainly related to the formation of gel hydration products of the geopolymerization process. The second exothermic peak decreases with increasing SS content due to the lesser calcium silicate phase in SS. In the deceleration stage, the effect of steel slag on the exotherm rate of the geopolymer gradually disappears, and the curves converge again. Fig. 3b shows the cumulative heat curve, which shows that a large amount of steel slag reduces the heat of reaction.

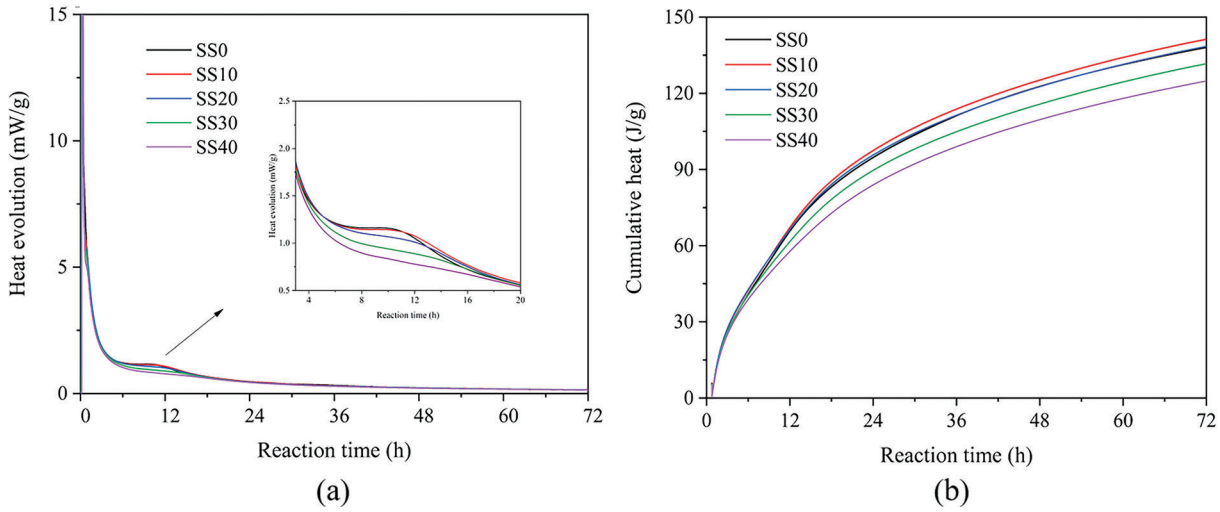

Figure 3: The heat of hydration curves of the geopolymer pastes (a) heat evolution, (b) cumulative hydration heat

4.2 Flowability

The flowability of geopolymer pastes with different SS levels is shown in Fig. 4. It can be seen from the figure that the flow value of the geopolymer pastes is gradually enlarged with the usage level of SS. The pure blast furnace slag has a minimum flow value of 170 mm. With the increase in SS content, the flowability of the geopolymer pastes increased by 2.9%, 10.6%, 14.7% and 20.6%, respectively, compared to the control group. The changes in the flow values may be caused by the higher content of amorphous material in BFS, which has higher pozzolanic activity and rapid hydration in the presence of alkali activator. Thus the degree of reaction of the geopolymer pastes with high BFS content is more intense to require more water. However, SS has more inert material. Thus, the addition of SS will decelerate the reaction process of the pastes and decrease the water requirement. Therefore, the geopolymer pastes containing SS have greater flowability.

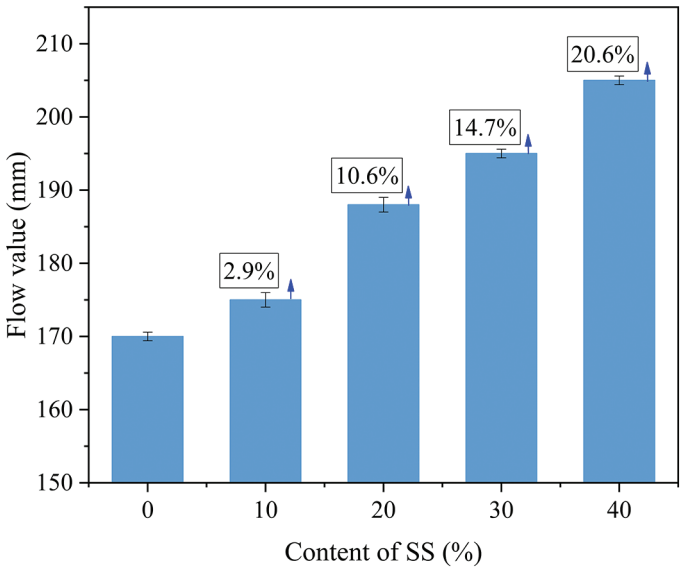

Figure 4: Effect of SS content on the flowability of fresh geopolymer pastes

4.3 Compressive Strength

The compressive strength of geopolymers with varying SS contents is shown in Fig. 5. It can be seen from the figure that the compressive strength of all specimens increased significantly with the increase of curing time. With the increase of SS content, the compressive strength at different curing ages showed an increasing trend followed by a decreasing trend. The compressive strength of the geopolymer paste with 10% SS content increased in different degrees compared with the control group at all ages. The compressive strength started to decrease when the SS content beyond 10%, and the compressive strength of the paste containing 20% SS was basically the same compared with the control group, while the early strength of the paste containing 30% SS and 40% SS both decreased greatly, by 28% and 34%, respectively, compared with the control group. It indicated that the addition of SS had a negative effect on the early compressive strength of the geopolymer, which may be caused by the low early activity of SS with low active components. Specifically, the reduction in early compressive strength was due to an incomplete geopolymerization process in which Al_2O_3 exhibited a high dissolution rate in the early stage, and therefore the low content of Al_2O_3 in SS (as shown in Table 1) could be the reason for the decrease in compressive strength [34]. With the increase of curing age, the compressive strength was further improved. Compared with the 3-day strength, the 28-day strength of the five groups of specimens increased by 6.94, 11.36, 8.6, 33.29, and 55.53 MPa, respectively. This demonstrates that the addition of SS facilitates the 28-day strength development due to the progressive accumulation of SS reactivity with increasing curing time, enhancing the geopolymer's later compressive strength growth. Furthermore, it is noteworthy that despite the addition of large amounts of SS, the compressive strength of the geopolymer paste containing 30% and 40% SS could still reach above 90% of the control samples at 28-day. This may be due to the Ca^{2+} content provided in the SS, which promotes more gels production and leads to increased strength.

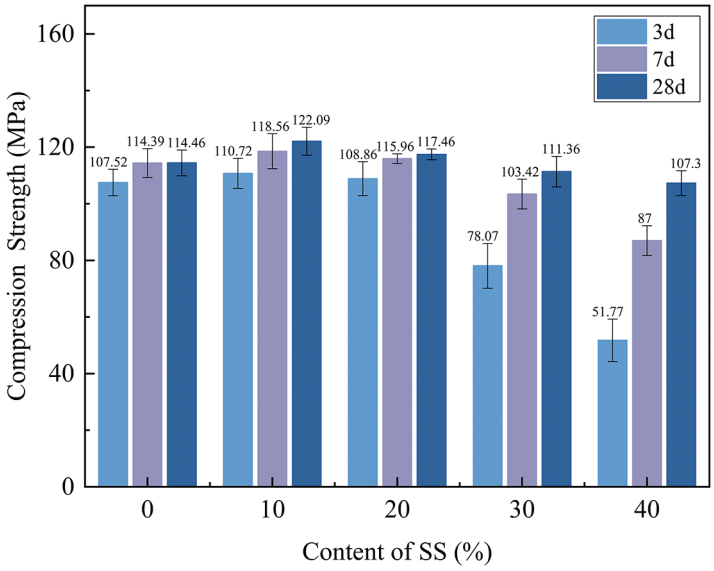

Figure 5: Compressive strength of samples with different SS content

4.4 Sorptivity Coefficient

The cumulative water absorption of the geopolymer specimens is shown in Fig. 6. It can be observed that the cumulative volume of water absorption for each unit of surface area (mm^3/mm^2) in the specimen increases with the square root of time. The cumulative water absorption of the geopolymer specimens was smaller than that of the control when the SS content was less than 20%. This means that the lower water absorption indicates smaller pores that are unable to absorb water, which may be related to the use

of moderate volumes of SS, resulting in a denser and stronger matrix. However, the cumulative water absorption increases with increasing SS content when the SS content is beyond 20%. The reason is that excessive SS leads to loose and porous microstructures, and these pores result in rapid water absorption of the geopolymer specimens. In combination with the above strength analysis results, the higher strength hardened geopolymer specimens typically exhibit lower adsorption coefficients, similar to other studies. This indicates that there is a limit value of SS content (20%), beyond which the hardened properties of the geopolymer are negatively affected. The relationship between the compressive strength and the sorptivity coefficient of the 28-day geopolymer is shown in Fig. 7 and fitted with a linear regression, and the Eq. (2) can be obtained as follows:

$$k = 0.76 - 4.11 \times 10^{-4} f, R^2 = 0.97 \tag{2}$$

where k = water absorption coefficient (mm/min$^{1/2}$), f = compressive strength (MPa).

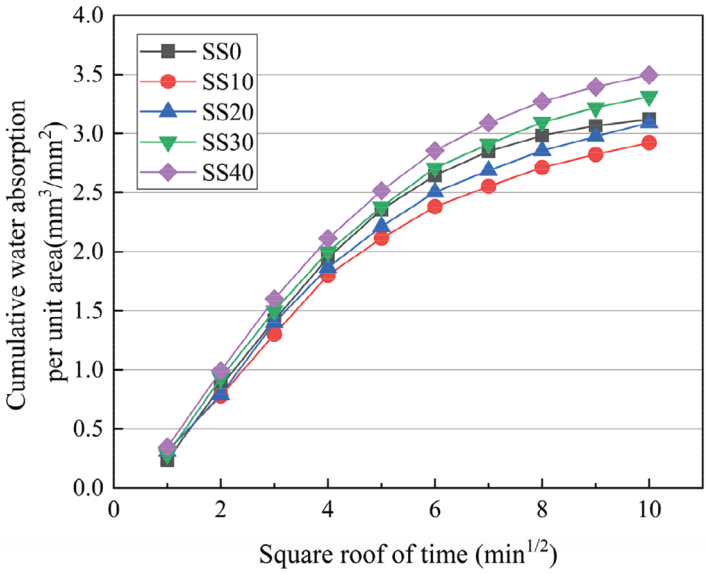

Figure 6: Typical result of water absorption as a function of time

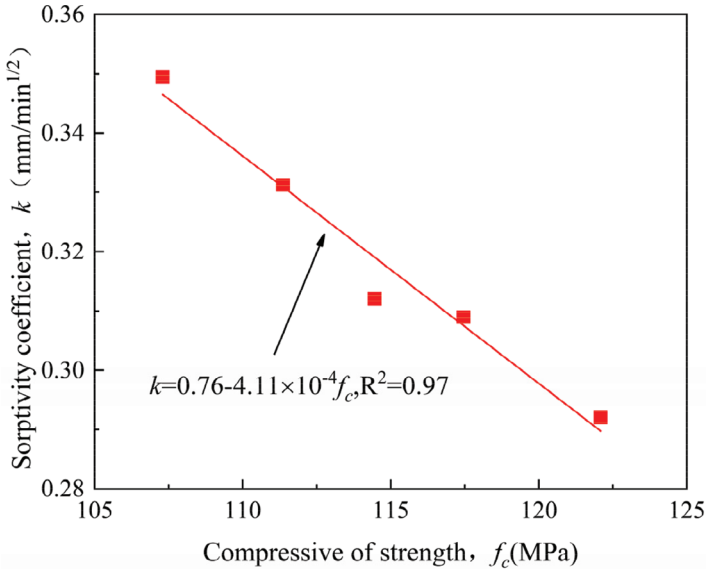

Figure 7: Relationship between water absorption coefficient and compressive strength of samples

4.5 Microstructural Properties

4.5.1 Characterization by XRD

Fig. 8 shows the XRD patterns of BFS, SS, and geopolymers with different SS contents at the curing age of 28 d. It can be seen that the BFS image shows a broad diffraction background hump near 30° (2θ), indicating that the BFS consists mainly of the amorphous phase, while the composition in the steel slag is more complex. Generally, the increase of SS has almost no effect on the main characteristic peaks of the geopolymer, and its main crystalline phase is quartz (SiO_2), which is mostly from BFS in combination with the XRD pattern of the raw material. However, the peak intensities of some quartz phases are diminished compared to the XRD patterns of the BFS, indicating that no or only a small portion of quartz was involved in the geopolymerization. Due to the higher peak of quartz, the other peaks of the geopolymer were less obvious, and some peaks of the raw materials were retained in the corresponding plots, but the intensities were all reduced. In addition to the crystal diffraction peaks, the presence of a large amount of amorphous material exists between 25°–35° (2θ), identified as C-(A)-S-H gels, with no decrease in the intensity of the gel peaks for SS20 and SS40 compared to SS0, suggesting that SS is involved in the hydration reaction and promotes the formation of gels. After the incorporation of SS, the 30°–35° (2θ) sharp peaks increased, and the wide peak area decreased slightly, and the changes were more obvious with the increase of SS. These results indicated that the geopolymer incorporated with SS forms new crystalline phases and reduces the amorphous components. It indicated that the hydration products of 20% SS content geopolymer had no significant influence compared with the control group, while the reaction degree and product amount of geopolymer was significantly impacted when the SS content was 40%.

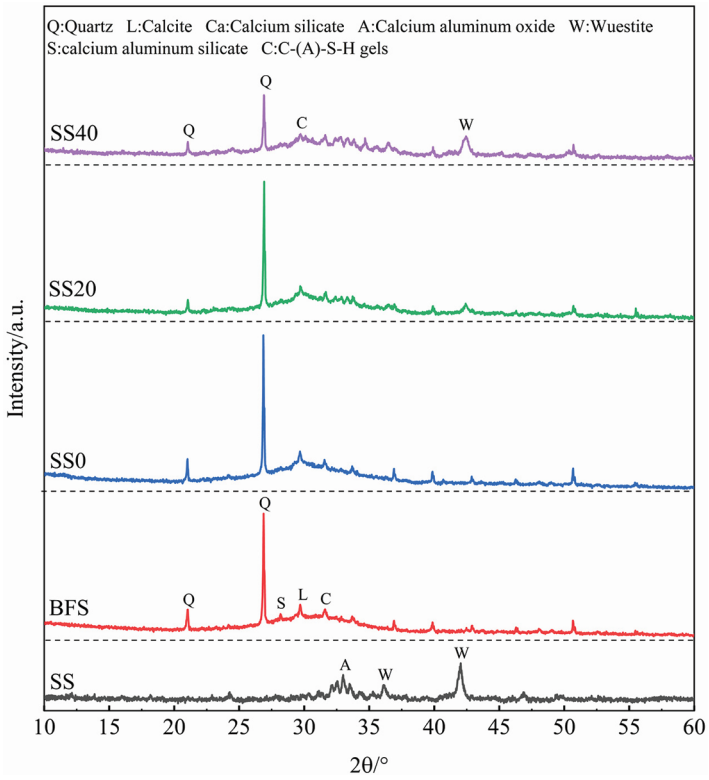

Figure 8: XRD patterns of SS, BFS and three geopolymer samples at 28 d

4.5.2 Characterisation by SEM

In order to reveal the impact of varying SS content on the microstructure of blast furnace slag based geopolymer, control groups SS0, SS20 and SS40 were selected for observation. Figs. 9a and 9b show the SEM images of the control group SS0. As can be seen, the microstructure of the control group includes geopolymer gels, pores, cracks, and unreacted slag particles, and the gel wrapping the unreacted large particles forms a relatively dense microstructure. In addition, some cracks are observed in the figures, which may have been formed during the preparation of the SEM specimen. Figs. 9c–9f show SEM images of SS20 and SS40 specimens, the cracks and micropores in the microstructure of the geopolymer were significantly reduced, and the SS particles and the gel were relatively tightly bound, which improved the mechanical strength of the geopolymer. However, the high SS content increases the pores of the geopolymer matrix, and observation of the SEM images of SS40 reveals that the samples are less dense and have a looser structure compared to SS0 and SS20, in agreement with the previous compressive strength results. This may be related to the nature of SS, where most of the large SS particles act as inert fillers and only the small size fine particles have high activity, so the large amount of SS leads to higher porosity and more harmful pores. Therefore, the addition of SS in an appropriate amount can effectively improve the microstructure compactness of geopolymer specimens, and the mechanical properties of geopolymer can be improved.

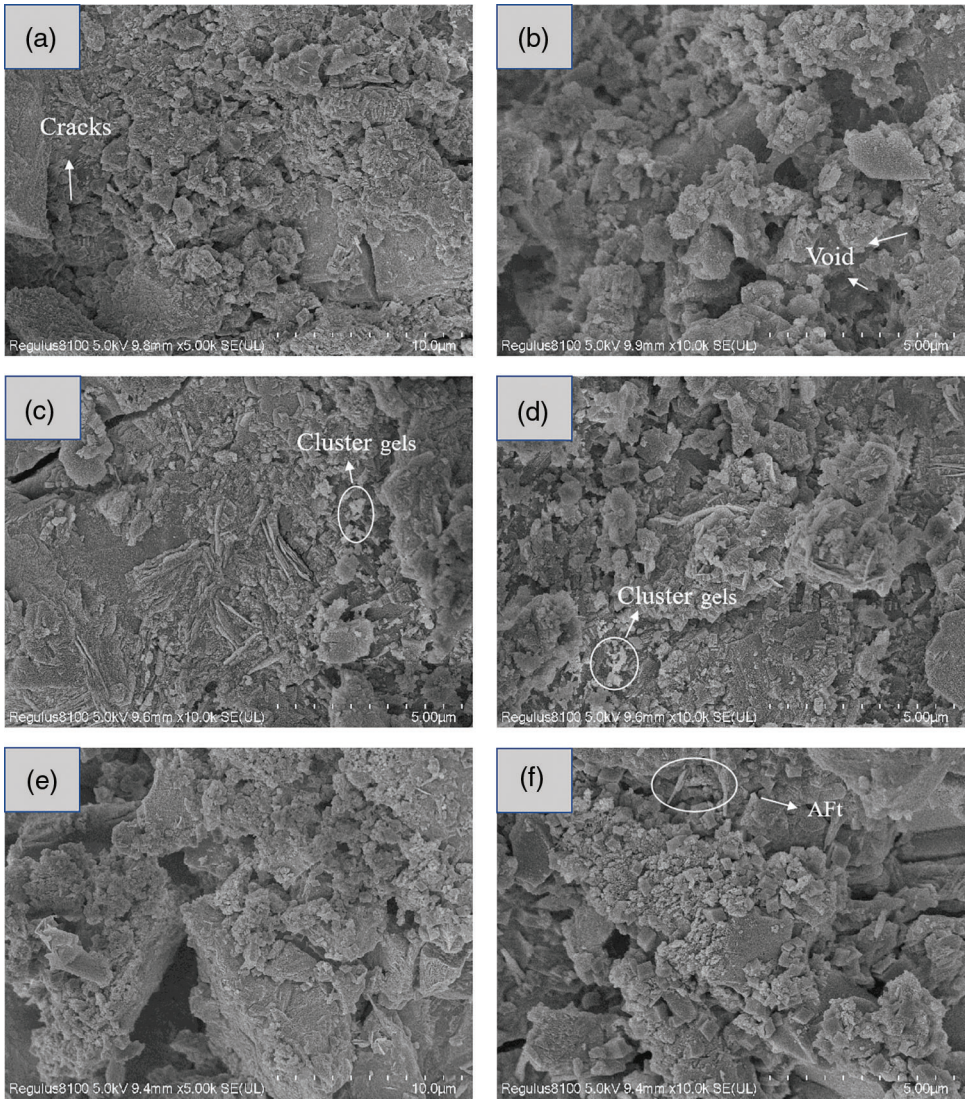

Figure 9: SEM images of samples at 28 d (a)–(b) SS0, (c)–(d) SS20, (e)–(f) SS40

5 Conclusions

This study investigates the potential of utilizing steel slag (SS) as a supplementary material in blast furnace slag-based geopolymer composite, and the experimental results obtained are summarized as follows:

1. SS has different effects on the exothermic rate during each hydration period. The addition of SS will reduce the area of the second peak, and too much SS will decrease the heat of reaction, which is not conducive to geopolymerization.
2. Since SS contains more inert substances, the addition of SS reduces the degree of reaction of the matrix and decreases the water requirement. Therefore, the addition of SS improves the flowability of the geopolymer paste, and the greater the SS content, the better the flowability of the geopolymer paste.
3. The compressive strength of the geopolymer paste at all ages increased and then decreased as the SS content gradually increased. It was observed that the addition of SS had a stronger effect on the early compressive strength and a less negative effect on the 28 d compressive strength. Even with the addition of a large amount of SS, the strength was still above 90% of that of the control group.
4. XRD and SEM show that the major product formed during the geopolymerization process was geopolymer gels with amorphous structures, which confirms the occurrence of the geopolymerization reaction. Although the addition of large amounts of SS reduced the reactivity of the matrix and reduced the geopolymerization, the gel products overlapped the surface of the residual particles, showing good mutual binding and reflecting high strength values.

Funding Statement: This work was supported by the Priority Academic Program Development of Jiangsu Higher Education Institutions (PAPD).

Conflicts of Interest: The authors declare that they have no conflicts of interest to report regarding the present study.

References

1. Hanjitsuwan, S., Phoo-ngernkham, T., Li, L., Damrongwiriyanupap, N., Chindaprasirt, P. (2018). Strength development and durability of alkali-activated fly ash mortar with calcium carbide residue as additive. *Construction and Building Materials, 162,* 714–723. https://doi.org/10.1016/j.conbuildmat.2017.12.034
2. Farhan, K. Z., Johari, M. A. M., Demirboğa, R. (2020). Assessment of important parameters involved in the synthesis of geopolymer composites: A review. *Construction and Building Materials, 264,* 120276. https://doi.org/10.1016/j.conbuildmat.2020.120276
3. Zakka, W. P., Abdul Shukor Lim, N. H., Chau Khun, M. (2021). A scientometric review of geopolymer concrete. *Journal of Cleaner Production, 280,* 124353. https://doi.org/10.1016/j.jclepro.2020.124353
4. Toniolo, N., Boccaccini, A. R. (2017). Fly ash-based geopolymers containing added silicate waste. A review. *Ceramics International, 43(17),* 14545–14551. https://doi.org/10.1016/j.ceramint.2017.07.221
5. Wang, Y., Dai, J., Wang, L., Tsang, D. C. W., Poon, C. S. (2018). Influence of lead on stabilization/solidification by ordinary portland cement and magnesium phosphate cement. *Chemosphere, 190,* 90–96. https://doi.org/10.1016/j.chemosphere.2017.09.114
6. Guo, X. S. H. W. (2017). Pore properties, inner chemical environment, and microstructure of nano-modified CFA-WBP (class C fly ash-waste brick powder) based geopolymers. *Cement and Concrete Composites, 79,* 53–61. https://doi.org/10.1016/j.cemconcomp.2017.01.007
7. Zheng, L., Wang, C., Wang, W., Shi, Y., Gao, X. (2011). Immobilization of MSWI fly ash through geopolymerization: Effects of water-wash. *Waste Management, 31(2),* 311–317. https://doi.org/10.1016/j.wasman.2010.05.015

8. Zhu, H., Liang, G., Xu, J., Wu, Q., Du, J. (2019). Surface-modification of fly ash and its effect on strength and freezing resistance of slag based geopolymer. *Construction and Building Materials, 199,* 574–580. https://doi.org/10.1016/j.conbuildmat.2018.12.059
9. McLellan, B. C., Williams, R. P., Lay, J., van Riessen, A., Corder, G. D. (2011). Costs and carbon emissions for geopolymer pastes in comparison to ordinary portland cement. *Journal of Cleaner Production, 19(9–10),* 1080–1090. https://doi.org/10.1016/j.jclepro.2011.02.010
10. Provis, J. L., van Deventer, J. S. J. (2007). Geopolymerisation kinetics. 2. Reaction kinetic modelling. *Chemical Engineering Science, 62(9),* 2318–2329. https://doi.org/10.1016/j.ces.2007.01.028
11. Cho, Y., Yoo, S., Jung, S., Lee, K., Kwon, S. (2017). Effect of Na_2O content, SiO_2/Na_2O molar ratio, and curing conditions on the compressive strength of FA-based geopolymer. *Construction and Building Materials, 145,* 253–260. https://doi.org/10.1016/j.conbuildmat.2017.04.004
12. Zhang, P., Gao, Z., Wang, J., Guo, J., Hu, S. et al. (2020). Properties of fresh and hardened fly ash/slag based geopolymer concrete: A review. *Journal of Cleaner Production, 270,* 122389. https://doi.org/10.1016/j.jclepro.2020.122389
13. Liang, G., Zhu, H., Li, H., Liu, T., Guo, H. (2021). Comparative study on the effects of rice husk ash and silica fume on the freezing resistance of metakaolin-based geopolymer. *Construction and Building Materials, 293,* 123486. https://doi.org/10.1016/j.conbuildmat.2021.123486
14. Hossain, S. S., Roy, P. K., Bae, C. (2021). Utilization of waste rice husk ash for sustainable geopolymer: A review. *Construction and Building Materials, 310,* 125218. https://doi.org/10.1016/j.conbuildmat.2021.125218
15. Bai, C., Deng, Y., Zhou, Q., Deng, G., Yang, T. et al. (2022). Effect of different curing methods on the preparation of carbonized high-titanium slag based geopolymers. *Construction and Building Materials, 342,* 128023. https://doi.org/10.1016/j.conbuildmat.2022.128023
16. Chen, J., Xing, Y., Wang, Y., Zhang, W., Guo, Z. et al. (2022). Application of iron and steel slags in mitigating greenhouse gas emissions: A review. *Science of the Total Environment, 844,* 157041. https://doi.org/10.1016/j.scitotenv.2022.157041
17. Chen, Y., Zhou, X., Wan, S., Zheng, R., Tong, J. et al. (2019). Synthesis and characterization of geopolymer composites based on gasification coal fly ash and steel slag. *Construction and Building Materials, 211,* 646–658. https://doi.org/10.1016/j.conbuildmat.2019.03.292
18. Hino, M. H. M. (2003). Enhancement of photosynthetic CO_2 fixation by marine phytoplankton with steelmaking slag as a nutrient source. *Tetsu-to-hagané, 89(4),* 381. https://doi.org/10.2355/tetsutohagane1955.89.4_381
19. Hayashi, A., Watanabe, T., Kaneko, R., Takano, A., Takahashi, K. et al. (2013). Decrease of sulfide in enclosed coastal sea by using steelmaking slag. *ISIJ International, 53(10),* 1894–1901. https://doi.org/10.2355/isijinternational.53.1894
20. Hayashi, A., Asaoka, S., Watanabe, T., Kaneko, R., Takahashi, K. et al. (2014). Mechanism of suppression of sulfide ion in seawater using steelmaking slag. *ISIJ International, 54(7),* 1741–1748. https://doi.org/10.2355/isijinternational.54.1741
21. Kong, Y., Wang, P., Liu, S. (2018). Microwave pre-curing of portland cement-steel slag powder composite for its hydration properties. *Construction and Building Materials, 189,* 1093–1104. https://doi.org/10.1016/j.conbuildmat.2018.09.088
22. Shi, M. X., Wang, Q., Zhou, Z. K. (2015). Comparison of the properties between high-volume fly ash concrete and high-volume steel slag concrete under temperature matching curing condition. *Construction and Building Materials, 98,* 649–655. https://doi.org/10.1016/j.conbuildmat.2015.08.134
23. Patil, S. V., Karikatti, V. B., Chitawadagi, M. (2018). Granulated blast-furnace slag (GGBS) based geopolymer concrete-review. *International Journal of Advanced Science and Engineering, 5(1),* 879–885. https://doi.org/10.29294/IJASE.5.1.2018.789-885
24. Saludung, A., Azeyanagi, T., Ogawa, Y., Kawai, K. (2023). Mechanical and microstructural evolutions of fly ash/slag-based geopolymer at high temperatures: Effect of curing conditions. *Ceramics International, 49(2),* 2091–2101. https://doi.org/10.1016/j.ceramint.2022.09.175

25. Liu, M., Wang, C., Wu, H., Yang, D., Ma, Z. (2022). Reusing recycled powder as eco-friendly binder for sustainable GGBS-based geopolymer considering the effects of recycled powder type and replacement rate. *Journal of Cleaner Production, 364,* 132656. https://doi.org/10.1016/j.jclepro.2022.132656
26. Huo, W., Zhu, Z., Sun, H., Gao, Q., Zhang, J. et al. (2022). Reaction kinetics, mechanical properties, and microstructure of nano-modified recycled concrete fine powder/slag based geopolymers. *Journal of Cleaner Production, 372,* 133715. https://doi.org/10.1016/j.jclepro.2022.133715
27. Lv, H., Chen, Y., Xie, Q., Wu, P., Chen, Y. et al. (2022). Performance optimization and characterization of loess-slag-based geopolymer composite: A new sustainable green material for backfill. *Construction and Building Materials, 354,* 129103. https://doi.org/10.1016/j.conbuildmat.2022.129103
28. GB/T 12959-2008 (2008). Test methods for heat of hydration of cement. National Standards of People's Republic of China, China.
29. GB/T 8077-2012 (2012). Methods for testing uniformity of concrete admixture. National Standards of People's Republic of China, China.
30. GB/T 17671-1999 (1999). Method of testing cements-determination of strength. National Standards of People's Republic of China, China.
31. ASTM C1585 (2011). Standard test method for measurement of rate of absorption of water by hydraulic-cement concretes. C1585. West Conshohocken, PA.
32. Sun, J., Chen, Z. (2019). Effect of silicate modulus of water glass on the hydration of alkali-activated converter steel slag. *Journal of Thermal Analysis and Calorimetry, 138(1),* 47–56. https://doi.org/10.1007/s10973-019-08146-3
33. Bernal, S. A., Provis, J. L., Rose, V., Mejía de Gutierrez, R. (2011). Evolution of binder structure in sodium silicate-activated slag-metakaolin blends. *Cement and Concrete Composites, 33(1),* 46–54. https://doi.org/10.1016/j.cemconcomp.2010.09.004
34. Mohd Ariffin, M. A., Hussin, M. W., Rafique Bhutta, M. A. (2011). Mix design and compressive strength of geopolymer concrete containing blended ash from agro-industrial wastes. *Advanced Materials Research, 339,* 452–457. https://doi.org/10.4028/www.scientific.net/AMR.339.452